END

FILMED

DTIC

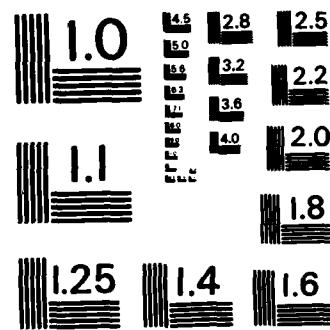MICROCOPY RESOLUTION TEST CHART

NATIONAL BUREAU OF STANDARDS-1963-A

⑫

Effects of Crystallite Orientation on the Oxidation of MoS$_2$ Thin Films

PAUL D. FLEISCHAUER and THOMAS B. STEWART
Chemistry and Physics Laboratory
Laboratory Operations
The Aerospace Corporation
El Segundo, CA 90245

9 September 1985

DTIC
ELECTE
S OCT 29 1985 **D**

B

Prepared for
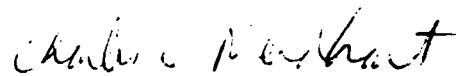
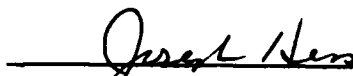This report was submitted by The Aerospace Corporation, El Segundo, CA 90245, under Contract No. F04701-83-C-0084 with the Space Division, P.O. Box 92960, Worldway Postal Center, Los Angeles, CA 90009-2960. It was reviewed and approved for The Aerospace Corporation by S. Feuerstein, Director, Chemistry and Physics Laboratory. Lieutenant Charles C. Neidhart was the project officer for the Mission-Oriented Investigation and Experimentation (MOIE) program.

This report has been reviewed by the Public Affairs Office (PAS) and is releasable to the National Technical Information Service (NTIS). At NTIS, it will be available to the general public, including foreign nationals.

This technical report has been reviewed and is approved for publication. Publication of this report does not constitute Air Force approval of the report's findings or conclusions. It is published only for the exchange and stimulation of ideas.

CHARLES C. NEIDHART, Lt, USAF
MOIE Project Officer
SD/CGX

JOSEPH HESS, GM-15
Director, AFSTC West Coast Office
AFSTC/WCO OL-AB

SECURITY CLASSIFICATION OF THIS PAGE *(When Data Entered)*

REPORT DOCUMENTATION PAGE		READ INSTRUCTIONS BEFORE COMPLETING FORM
1. REPORT NUMBER SD-TR-85-63	2. GOVT ACCESSION NO. AD-A160 617	3. RECIPIENT'S CATALOG NUMBER
4. TITLE *(and Subtitle)* EFFECTS OF CRYSTALLITE ORIENTATION ON THE OXIDATION OF MoS$_2$ THIN FILMS		5. TYPE OF REPORT & PERIOD COVERED
		6. PERFORMING ORG. REPORT NUMBER TR-0084A(5945-03)-2
7. AUTHOR(s) Paul D. Fleischauer and Thomas B. Stewart		8. CONTRACT OR GRANT NUMBER(s) F04701-83-C-0084
9. PERFORMING ORGANIZATION NAME AND ADDRESS The Aerospace Corporation El Segundo, CA 90245		10. PROGRAM ELEMENT, PROJECT, TASK AREA & WORK UNIT NUMBERS
11. CONTROLLING OFFICE NAME AND ADDRESS Space Division Los Angeles Air Force Station Los Angeles, CA 90009-2960		12. REPORT DATE 9 September 1985
		13. NUMBER OF PAGES 22
14. MONITORING AGENCY NAME & ADDRESS*(if different from Controlling Office)*		15. SECURITY CLASS. *(of this report)* Unclassified
		15a. DECLASSIFICATION/DOWNGRADING SCHEDULE

16. DISTRIBUTION STATEMENT *(of this Report)*

Approved for public release; distribution unlimited.

17. DISTRIBUTION STATEMENT *(of the abstract entered in Block 20, if different from Report)*

18. SUPPLEMENTARY NOTES

19. KEY WORDS *(Continue on reverse side if necessary and identify by block number)*

Molybdenum disulfide
Solid lubrication
Thin-film chemistry
Thin-film oxidation
Crystallite orientation

20. ABSTRACT *(Continue on reverse side if necessary and identify by block number)*

Thin films of MoS$_2$ have been prepared, by rf sputter deposition, with different microstructures that show markedly different susceptibilities to oxidation or other environmental degradation. The films were exposed to air atmospheres of variable relative humidity, and the extent of oxidation was measured by means of Auger electron (AES) and X-ray photoelectron (XPS) spectroscopies. The morphologies of the films were determined by transmission electron microscopy. Depths of oxidation of the thin films

DD FORM 1473
(FACSIMILE)

19. KEY WORDS (Continued)

20. ABSTRACT (Continued)

were calculated from changes in AES peak-to-peak height ratios and in XPS peak intensity ratios through the use of standard escape-depth models for attenuation of electron emission by a layer of reacted material (in the present case, MoO_3). The results show that MoS_2 films whose crystallites are oriented with their basal planes at random angles to the plane of the substrate surface (designated Type I films) are oxidized to depths equal to or greater than 300 Å, whereas films whose crystallite basal planes are coplanar with (parallel to) the substrate surface (Type II films) are oxidized to a maximum depth of 10 to 15 Å. These results are interpreted in terms of the relative reactivities of edge versus basal planes of the MoS_2 crystallites. Keywords:

PREFACE

We are grateful to R. I. Christy of Hughes Aircraft Company for preparing the films. We also thank S. A. Jackson and J. L. Childs for measuring the AES and XPS spectra, respectively.

CONTENTS

A-1

3

FIGURES

TABLES

I. INTRODUCTION

The reactivities in humid and dry atmospheres of thin films of molybdenum disulfide prepared by rf sputtering were recently found to be substantially greater than that of the bulk (powder) material.[1] The nature of the oxidation reaction at room temperature for the thin films (~2000 Å thick) was determined to be conversion from MoS_2 to MoO_3 with no evidence of sulfite or sulfate species on the film surfaces in agreement with the similar reaction that occurs on the powder.[2] The reported depths of film oxidation were estimated to be in excess of 100 Å from empirical correlations of the changes in peak-to-peak heights of Auger electron spectra to changes in MoS_x stoichiometry (i.e., S:Mo atom ratios). Those changes in the films' chemistries were then correlated to variations in their tribological (lubrication) properties under conditions of sliding contact between lubricated surfaces. Oxidation of the MoS_2 films completely destroyed their desirable lubrication qualities, reducing their wear lives by a factor of 50 or more.

Subsequently, MoS_2 films have been produced, by the same rf sputtering technique, that have considerably different chemical and tribological properties.[3] Those films exhibit very little oxidation under more severe conditions than those reported previously; under no standard environmental conditions (i.e., varying relative humidity at room temperature) are the newer films oxidized to any significant depth (>10-15 Å). Auger and X-ray photoelectron spectroscopy data for all of the MoS_2 films have been fit to a model describing the surface oxidation process. The results of depth-of-oxidation calculations based on that idealized model are presented here. The differences in the reactivities of the two types of films and the influence of crystallite orientation on reactivity are then discussed.

7

II. EXPERIMENTAL SECTION

MoS_2 films were prepared by rf sputtering according to the same procedures as described previously.[1,3] Two different sputtering targets were used, one from Materials Research Corporation that produced the first set of films with the relatively high reactivities,[1] and the other from Cerac, Inc., that produced the second relatively inert set.[3] Both targets were made from hot-pressed MoS_2 powder (99.9% pure), and the sputtering parameters (i.e., rf power, argon pressure) were the same regardless of which target was used. Films were made on primarily C1018 or 440C steel substrates and were ~2000 Å thick. A few depositions of ~750-Å-thick films were done onto carbon-coated copper transmission electron microscope grids.

Following their preparation, films were stored in various environments (air of different relative humidity) for times ranging from 2 weeks to 16 months. Films were stored in crystallizing dishes over solutions that were used to maintain the appropriate relative humidity. Watch glasses were placed over the crystallizing dishes and the seams taped with electrical tape. The indicated relative humidities were maintained with the following saturated solutions: 51%--$Cu(NO_3)_2 \cdot 4H_2O$; 84%--KBr; 98%--$CaSO_4 \cdot 5H_2O$. In addition, some films were stored over distilled water (100% RH) and some in a desiccator over dry $CaSO_4$.

Auger electron spectroscopy (AES) was performed with a Physical Electronics Industries Model 590 scanning Auger microprobe, using the same operating conditions as previously described.[1] X-ray photoelectron spectra (XPS) were taken with a GCA/McPherson ESCA-36 spectrometer that had been modified by the addition of a position-sensitive, multichannel detector.[4] The modified detector system increases the signal-to-noise ratio and decreases considerably the time to obtain a spectrum. MoS_2 powder (ultrapure acid washed) and molybdenite single-crystal samples were analyzed as standards by both AES and XPS. The single crystals were obtained from Ward's Natural Science Establishment. They were cleaved with an X-acto knife immediately prior to AES or XPS analysis.

III. RESULTS

The oxidation chemistry of the sputtered MoS_2 thin films was studied by exposing the films to atmospheres of differing relative humidity for varying lengths of time and then analyzing the surface compositions by Auger electron or X-ray photoelectron spectroscopy. Considerable AES and XPS data on MoS_2 are available in the literature primarily because of MoS_2 use in catalysis[5-8] but also in connection with its lubrication properties.[9-11] The spectra for molybdenite are shown in Fig. 1. The samples were oriented so that excitation and emission occur on the basal planes of the hexagonal crystals. One of the objectives of this study is to prepare, for lubrication applications, MoS_2 thin films with spectra as close to those of the crystal as possible. As a general rule it appears that those films whose spectra are most like those of the basal plane of the crystal have the best lubrication properties and the greatest resistance to oxidation.

There are significant features in both the XPS and AES spectra that are indicative of the purity of the MoS_2 surface being analyzed. The presence of impurity peaks, of course, indicates oxidation or surface adsorption of, for example, carbon compounds. But, in this study, attention is paid to the shapes and intensities of the sulfur and molybdenum peaks and the information that such peaks can provide about the stoichiometry of the MoS_x as a function of depth into the film. The XPS spectrum of Fig. 1a shows the impressive quality of the 3d electron doublet for the crystal. The integrated intensity ratio for the $3d_{5/2}$ to $3d_{3/2}$ peaks is 1.55:1 in agreement with the theoretical prediction of 1.5:1. The peak-to-peak intensity ratio is approximately 1.8:1. The latter ratio, though slightly less accurate, is used subsequently to determine the degree of oxidation of the MoS_2 thin films because of its ease of determination.

Oxidation of MoS_2 to MoO_3 results in a second Mo 3d doublet shifted to higher binding energy by ~3 eV, which is also the value of the doublet splitting for MoS_2. The consequences of this shift are shown in Fig. 2, in particular Figs. 2b and 2d, where three Mo 3d peaks are observed, the middle
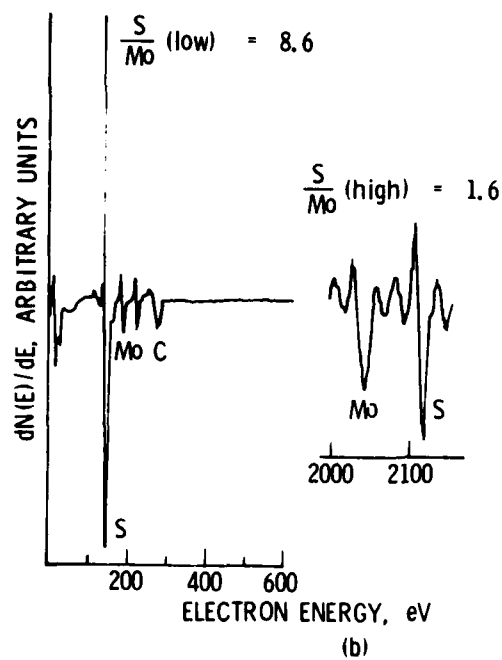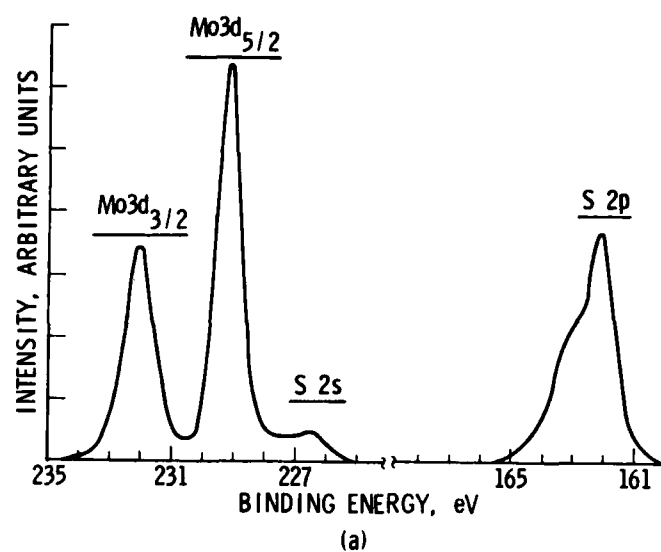
11

Fig. 1. (a) X-ray photoelectron spectrum of MoS_2 single crystal (molybdenite); (b) Auger spectrum of MoS_2 single crystal.
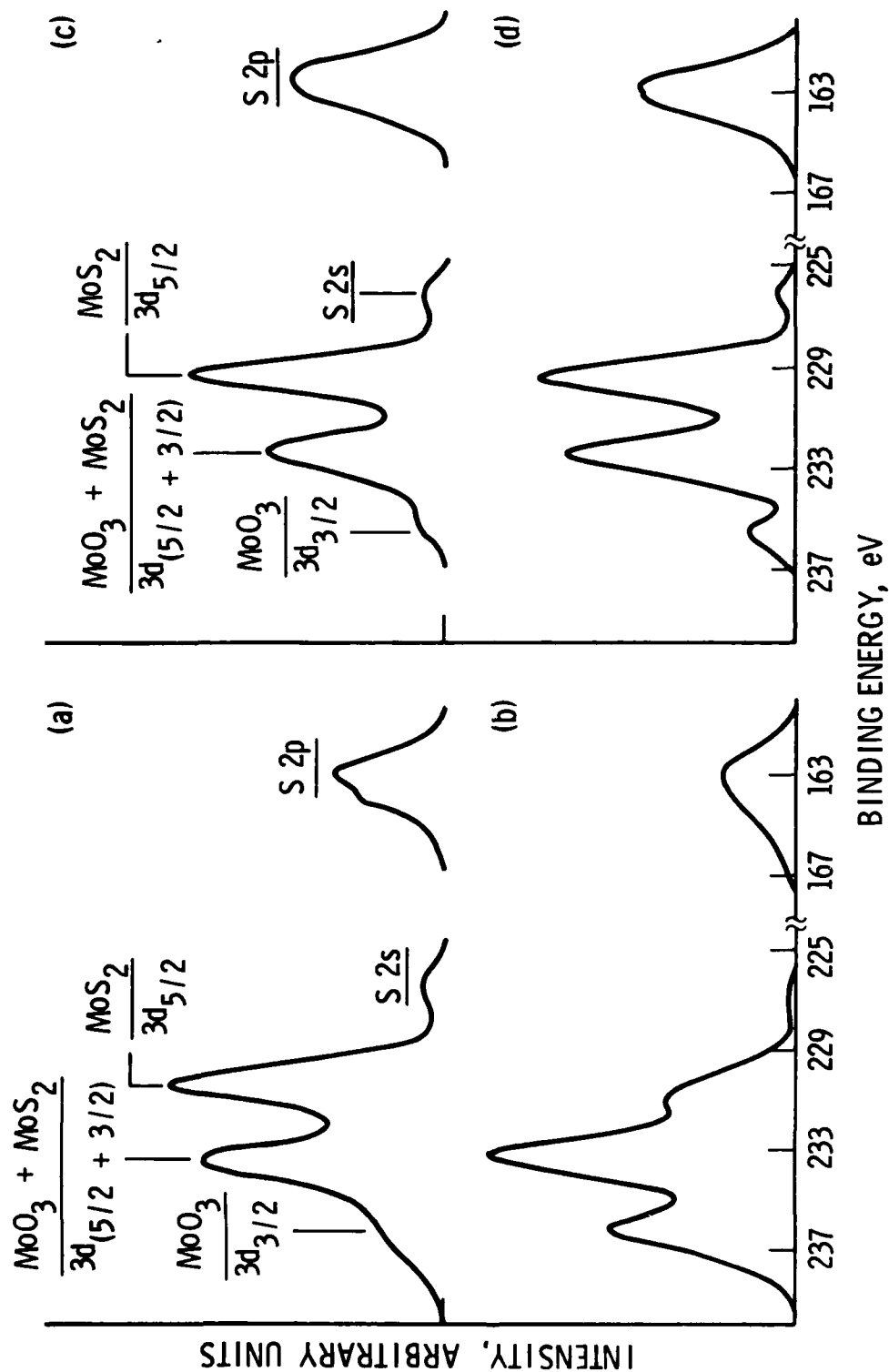
Fig. 2. XPS spectra of rf sputter-deposited MoS_2 thin films before and after storage in dry air, 0% RH: (a) fresh Type I film; (b) Type I after 9 months' storage; (c) fresh Type II film; and (d) Type II after 12 months' storage.

13

one corresponding to the overlap of the Mo(IV) $3d_{3/2}$ and the Mo(VI) $3d_{5/2}$ peaks. The extent of reaction of MoS_2 has been determined from spectra such as those of Fig. 2 by assuming that there are only two emitting Mo species, the Mo(IV) of MoS_2 and the Mo(VI) of MoO_3. The aforementioned peak ratios are used to resolve the middle composite peak, and the relative amounts of Mo(IV) and Mo(VI) are estimated and tabulated in Table I, column 5. (A film that is totally oxidized so that only the Mo(VI) peaks of MoO_3 are observed has a $3d_{5/2}:3d_{3/2}$ peak ratio of 1.51:1, which has been accounted for in the data of Table I.) In view of the broadening of the peaks, other molybdenum species have probably formed on the surfaces of the films. However, the trends in the data and the differences among various films are considered large enough to justify this method of interpreting relatively gross differences in the films and their reactivities.

The S peak for the single crystal (Fig. 1a) depicts the partial resolution of the S $2p_{3/2,1/2}$ doublet, the splitting here being only ~1 eV. The analogous peaks for the sputtered films are broadened and not well resolved. The extent of asymmetry of the S peak primarily on the high binding energy side varies from film batch to film batch. This S peak broadening is believed to be caused by the presence of elemental S in the sputtered films in a manner analogous to the situation observed for MoS_3.[7] (This compound is believed to be MoS_2 with elemental S interspersed in the crystal lattice.)

The Auger spectra of molybdenum-sulfur compounds are particularly useful for the determination of surface reactivities and reaction depths because of the fortunate occurrence of two sets of Mo and S peaks and the closeness of their respective energies. The sulfur LMM(LVV) and the molybdenum MNN peaks are at 151 and 186 eV, respectively, and the sulfur KLL and molybdenum LMM peaks are at 2117 and 2044 eV, respectively, as shown in Fig. 1b. Values of the peak-to-peak "intensity" ratios of the S to the Mo signals for the sputter-deposited films have been compared with the value for the molybdenite crystal to assess the magnitude of changes in MoS_x stoichiometry. (Various precautions, related to chemical shifts, and advantages of this procedure are reported in Ref. 1.) The oxidation reaction, that which produces Mo(VI) as observed in the XPS data, produces primarily volatile sulfur products and

14

Table I. Chemical Properties of Sputtered MoS_2 Films

Film Type/Conditions[a]	S:Mo(L)[b]	S:Mo(H)[c]	O:Mo(H)[d]	Mo(IV):Mo(VI)[e]
Type I				
initial	7.5	1.45	5.9	>3
0.5 month at 0% RH	8.0	1.25	5.9	~1.6
9 months at 0% RH	6.6	0.95	8.9	~0.6
1 month at 51% RH	6.9	1.08	9.4	~0.8
9 months at 51% RH	7.1	1.02	9.4	~0.6
9 months at 84% RH	5.5[f]	0.98[f]	13.2	<0.1
0.5 month at 98-100% RH	4.1	0.58	12.6	<0.1
Type II				
initial	9.0	1.6	1.2	>6
1 month at 0% RH	8.7	1.58	1.8	
2 months at 0% RH	7.6	1.53	1.9	
12 months at 0% RH	7.8	1.55	3.5	~3
1 month at 51% RH	9.2	1.55	2.6	~5
2 months at 51% RH	7.2	1.51	3.6	~2.5
1 month at 84% RH	6.8	1.37	3.8	
2 months at 84% RH	8.1	1.63	2.7	~2
1 month at 98% RH	8.8	1.52	2.7	
2 months at 98% RH	5.4	1.46	4.2	~1
MoS_2 powder	8.9	1.7	0	∞
MoS_2 crystal	8.5	1.64	0	∞

[a]RH = relative humidity, air atmosphere.
[b]AES peak-to-peak height ratios for low-energy sulfur and molybdenum peaks.
[c]AES ratios for high-energy peaks.
[d]AES ratios for oxygen peak at ~530 eV to Mo high-energy peak.
[e]Ratios of different Mo oxidation states obtained from XPS peak heights.
[f]Large values of S:Mo represent a surface of MoO_3 covered/mixed with polysulfur (S_8) as determined from S binding energy (164 eV) from XPS.

15

nonvolatile MoO_3. Therefore, changes in the S:Mo Auger peak-to-peak ratios indicate the extent of the oxidation process.[1]

The depth, beneath the film surface, from which an Auger electron or photoelectron escapes is a function of the energy of the electron.[12,13] The inelastic mean free path (IMFP) of the electron in the solid is a measure of the escape depth (λ). The dependence of λ on electron energy has been described with different functions; the one used for this work is an empirical fit[14] for inorganic solids and electron energies greater than 150 eV and is given by

$$\lambda(\text{Å}) = 0.96\ E^{0.5} \qquad (1)$$

A summary of the escape depths for the various electron emissions of significance for MoS_2 is presented in Table II. The values vary from ~10 Å for the low-energy S and Mo Auger peaks to over 40 Å for the high-energy Auger peaks.

Variations in the AES data for different MoS_2 films and for films stored under different conditions are shown in Fig. 3 and in Table I. Peak-to-peak height ratios for S and Mo peaks were calculated from spectra such as those in Fig. 3. Selected data are given in Table I, whereas data for numerous films are plotted in Fig. 4. It is clear from these data and from the XPS data that the sputter-deposited MoS_2 films fall into two distinctly different categories: one group that is relatively easily and substantially oxidized (designated Type I), and one that appears to be oxidized only at the outermost film surface (Type II). The S:Mo ratios for the Type I films decrease by 50 to 60% from their initial values, and there is almost no detectable Mo(IV) in the XPS for the most heavily oxidized films, those stored for 2 weeks at 98% RH. Conversely, the high-energy S:Mo AES ratios for the Type II films decrease by less than 15% and the Mo(IV):Mo(VI) ratio reaches a minimum value of ~1:1 for films stored up to 2 months at 98% RH. These data are interpreted in terms of a model, described in the following section, that is based on differences in depth of oxidation for the two film types. The lines drawn in Fig. 4 are calculated from the proposed model. The differences in depth of oxidation are attributed to differences in orientation of the crystallites

16

Table II. Inelastic Mean Free Paths of Electrons in MoS_2

Element	Process/Transition	Kinetic Energy (eV)	$\lambda(\text{Å})$[a]
Mo	Auger/MNN	186	13
Mo	Auger/LMM	2044	43
Mo	XPS/$3d_{5/2}$	1020	31
S	Auger/LMM	151	12
S	Auger/KLL	2117	44
S	XPS/$2p_{3/2}$	1086	32

[a]Based on Eq. (1) in text.
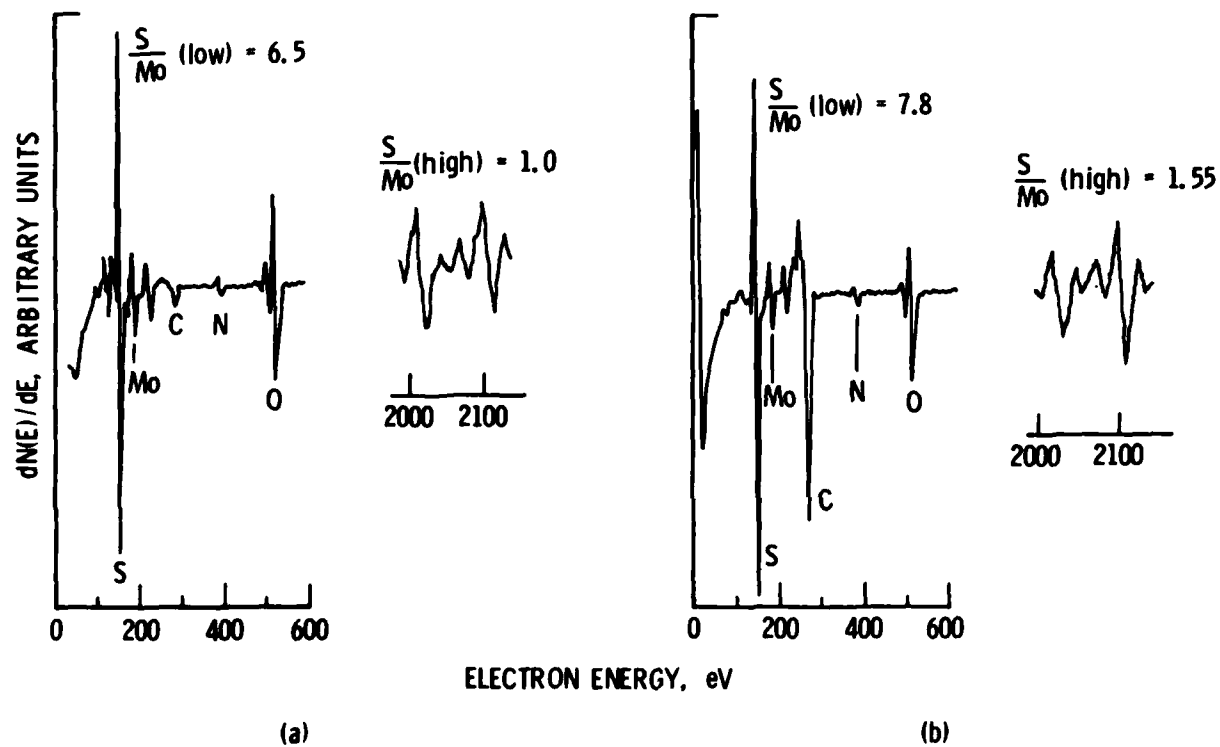
Fig. 3. Auger spectra of rf sputter-deposited MoS_2 thin films after 1 year of storage in dry air: (a) Type I film; (b) Type II film.
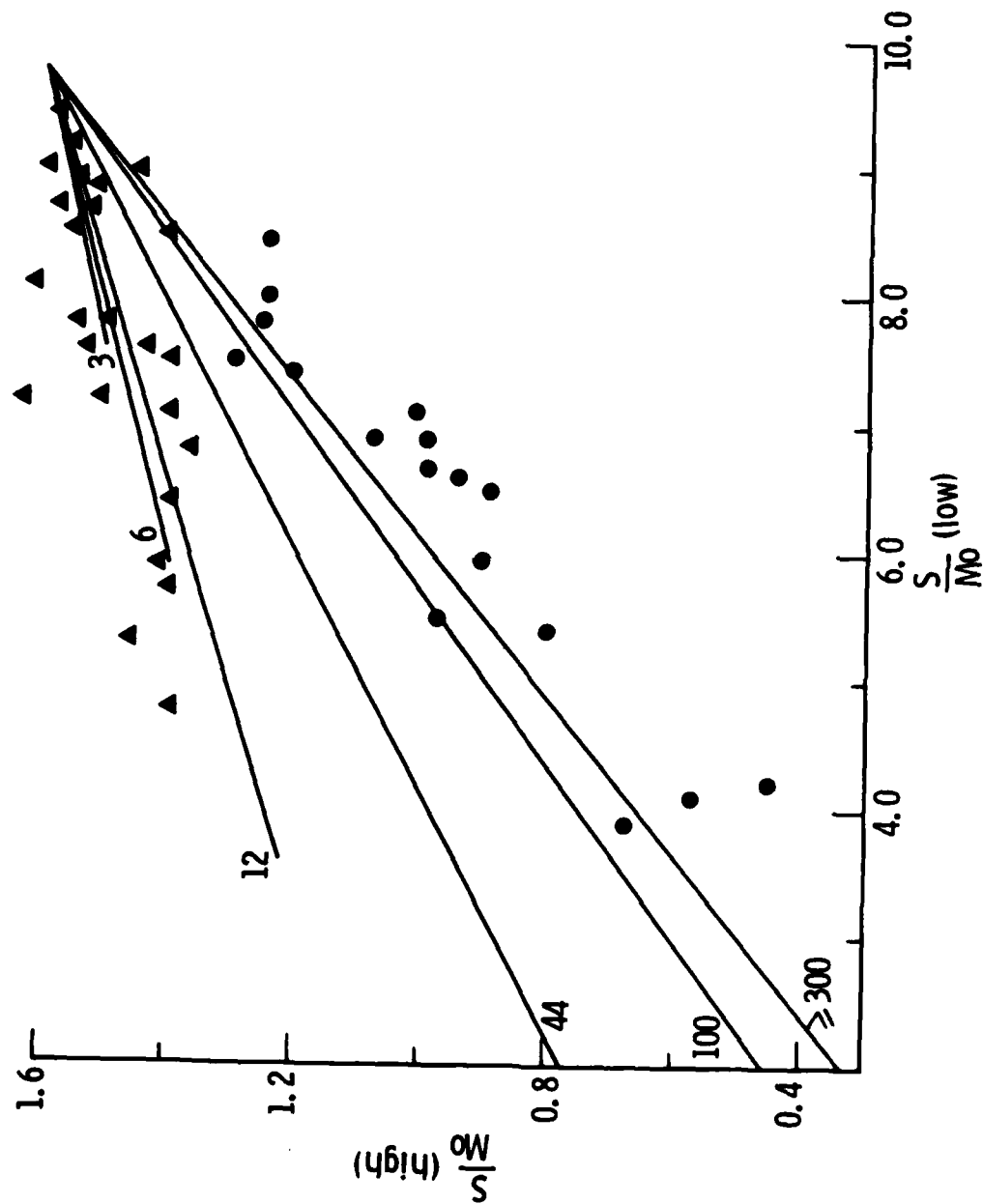
Fig. 4. Plots of ratios of Auger peak-to-peak heights for S and Mo. ● = Type I films, ▲ = Type II films. Lines are calculated from model of surface oxidation described in text. Numbers on lines refer to thickness (Å) of oxidized layer on MoS_2.

that make up the thin films. The transmission electron micrographs (TEM), shown in Fig. 5, depict a random orientation of crystallites with exposure of the edge planes to the outer surface for Type I films and a regular planar orientation with basal planes exposed for Type II films. The electron diffraction pattern for Type I films is diffuse with only carbon rings in evidence; the pattern for Type II films clearly displays the rings of MoS_2.

1000 Å

(b)

1000 Å

(a)
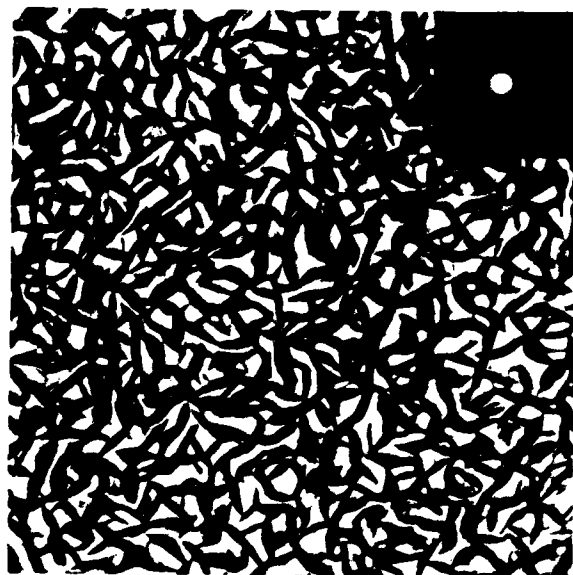
Fig. 5. Transmission electron micrographs of rf sputter-deposited MoS_2 films on carbon substrates. (a) Type I film, random crystallite orientation; (b) Type II film, parallel orientation. Shown in the corner of each micrograph are the electron diffraction patterns measured for that film.

21

IV. MODEL FOR SURFACE OXIDATION

Figure 6 presents a schematic of an idealized MoS_2 surface that is partially oxidized. This picture has been used to develop a simplified model of MoS_2 oxidation in an attempt to explain the data of Fig. 4. From the represented MoS_2 film (layer B) covered with a layer (A) of oxidized material of thickness $t(Å)$, the following assumptions were made to calculate variations in AES or XPS peak intensity ratios: (1) The thickness (t) of the oxidized layer was selected and held constant while the fraction of oxide in the layer was varied from 0 to 1. (2) The composition of the overlayer A was assumed to be limited to mixtures of just two compounds, MoS_2 and MoO_3; i.e., the sum of sulfide and oxide mole fractions always equalled one. (3) While the sulfide and oxide concentrations in layer A varied, the total Mo concentration remained constant. (4) The oxide and sulfide concentrations within layer A were assumed to be uniform throughout the entire layer. A more realistic model would incorporate a concentration gradient within the overlayer, but, because the assumption of uniform concentration produced very good fits to the data, further refinements in the calculations were not implemented. (5) The escape depths (λ) for the Auger electrons and photoelectrons were assumed to depend only on the electron energy [see Eq. (1)] and not on the composition of the overlayer.

The procedure for performing the calculations was to set an overlayer thickness and then calculate the S:Mo Auger peak intensity ratios relative to that of pure MoS_2 as a function of increasing oxide concentration. The calculations were done discretely for oxide concentrations of 10, 25, 50, 60, 70, 80, and 100 mol% and thickness t indicated on the lines in Fig. 4. A standard expression [Eq. (2)] was used to calculate the intensity of an emitted electron attenuated by an overlayer.[15] In the case of S,

$$I_S \propto X_S^A \lambda_S (1 - e^{-t/\lambda_S}) + X_S^B \lambda_S e^{-t/\lambda_S} \qquad (2)$$

23

t $MoO_3 + MoS_2$ A LAYER

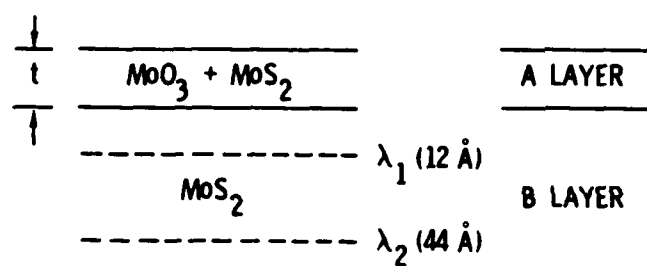λ_1 (12 Å)

MoS_2 B LAYER

λ_2 (44 Å)

Fig. 6. Schematic of oxidized layer on top of an MoS_2 film. Electron escape depths for the low- and high-energy Auger electrons from S and Mo are indicated.

where the proportionality includes terms for the ionization cross section of the electron ejected from the emitting atom by the incident excitation, parameters for the spectrometer, and the flux of incident radiation; the first term on the right side represents emission from layer A, where X_S^A is the fraction of sulfide in the layer and λ_S the escape depth for S electrons; and the second term represents emission from the bulk MoS_2 (layer B) attenuated by the overlayer A. A similar expression may be written for emission by Mo, but since the Mo concentration is assumed to be uniform regardless of oxidation, the intensity of Mo electron emission is equal to that for pure MoS_2. (Strictly speaking, this derivation holds for the Auger emission; a slightly different situation pertains to XPS, where relative amounts of Mo(IV) and Mo(VI) are calculated. For both, the value of t used in the appropriate equations must be corrected for the takeoff angle of the respective spectrometer.) If all the factors included in the proportionality of Eq. (2) and the preexponential λ are accounted for by setting them equal to I_S^o, the intensity of emission from pure MoS_2, the following expression for the ratio I_S/I_{Mo} may be written:

$$\frac{I_S}{I_{Mo}} = \frac{I_S^o}{I_{Mo}^o} \left[X_S^A (1 - e^{-t/\lambda}S) + e^{-t/\lambda}S \right] \tag{3}$$

Equation (3) was used to calculate values of the Auger peak intensity ratios for both low-energy (150-186 eV) and high-energy (2044-2117 eV) S and Mo peaks by selecting the proper λ from Table II and allowing X_S^A to vary as described previously. The lines drawn on Fig. 4 for oxide layer thicknesses ranging from 3 to > 300 Å result from these calculations. The calculated lines converge at t = 300 Å; the line for t = ∞ is essentially identical to that for t = 300 Å. The termini of the lines for t = 3, 6, and 12 Å represent the situation for 100% oxidation of the layers of those thicknesses. The lines do indeed stop rather than continue beyond those points. The data of Fig. 4 demonstrate that the Type I films are oxidized to depths of 300 Å or more, whereas, conversely, Type II films are oxidized to only ~10 to 12 Å.

The ability to obtain this type of depth-of-oxidation information results from the fact that sets of low- and high-energy Auger peaks exist for the

elements of interest—a somewhat rare occurrence but one that permits analysis of the surfaces to depths far exceeding the escape depths of the respective electrons.

The XPS data for Types I and II films corroborate the Auger data. Similar intensity expressions were used to calculate oxide layer thicknesses required to obtain the measured Mo(IV):Mo(VI) ratios. The Auger data for Type I films indicate that the most severely oxidized samples have 80 to 90% oxide to depths exceeding 300 Å. The XPS data suggest that the depths of oxidation for the same films are >150 Å, whereas the depths of oxidation for 100% oxidation for the Type II films are ~15 Å.

V. DISCUSSION

The data described in Section II and the calculations of Section IV point toward the occurrence of sputter-deposited MoS_2 films with widely differing reactivities, vis a vis oxidation, resulting from major differences in the structures and morphologies of the films. Spalvins has shown that sputtered MoS_2 films can be amorphous if deposited at low temperature and that only crystalline films are good lubricants.[11] Both types of films studied in this work are good lubricants (although Type II films are superior), but the Type II films have vastly superior resistance to oxidation prior to use.

We interpret these results to mean that the crystallites of Type II films are oriented parallel to the substrate surface immediately upon deposition, whereas those of Type I films are not oriented. The crystal structures of the individual platelets are probably hexagonal in both cases, but the platelets (crystallites) present either edge (Type I) or basal (Type II) faces to the reactive oxygen and water-vapor molecules of hostile environments. It is known that such gases will be adsorbed on the edge face of molybdenite but not on the basal plane.[8,9]

We conclude that the crystallite orientation of Type II films provides the observed resistance toward oxidation, because penetration to the Mo(IV) reaction sites can occur only at grain boundaries or at other imperfections in these films. The 10- to 15-Å depth of oxidation is equivalent to penetration of two to three crystallographic layers, the Mo-Mo spacing in the C-axis direction being 6.16 Å.[16] Other investigators have demonstrated that the crystallites of sputter-deposited MoS_2 films can be oriented by burnishing (rubbing) the films after preparation; the films' appearance changes from matte black to shiny, silvery black. However, to our knowledge this is the first case where the films come out of the sputtering chamber with the oriented configuration. We are still determining the preparation conditions that produce the planar versus the random configuration and expect them to be the subject of a subsequent report.

27

REFERENCES

1. T. B. Stewart and P. D. Fleischauer, Inorg. Chem. 21, 2426 (1982).

2. I. B. Atkinson and P. Swift, Wear 29, 129 (1974).

3. P. D. Fleischauer, ASLE Trans. 27, 82-88 (1984).

4. P. A. Bertrand, W. J. Kalinowski, L. E. Tribble, and L. U. Tolentino, Rev. Sci. Instrum. 54, 387 (1983).

5. T. A. Patterson, J. C. Carver, D. E. Leyden, and D. M. Hercules, J. Phys. Chem. 80, 1700 (1976). W. E. Swartz, Jr., and D. M. Hercules, Anal. Chem. 43, 1774 (1971).

6. M. Salmeron and G. A. Somorjai, Surf. Sci. 126, 410 (1983). S. J. Tauster, T. A. Pecoraro, and R. R. Chianelli, J. Catal. 63, 515 (1980).

7. G. C. Stevens and T. Edmonds, J. Catal. 37, 544 (1975).

8. K. Suzuki, M. Soma, T. Oniski, and K. Tamaru, J. Electron Spectrosc. Relat. Phenom. 24, 283 (1981).

9. M. Matsunaga, T. Homma, and A. Tanaka, ASLE Trans. 25, 323 (1982).

10. D. R. Wheeler, NASA Tech. Memo. NASA TM-78896 (1978).

11. T. Spalvins, Thin Solid Films 73, 291 (1980).

12. C. J. Powell, in Quantitative Surface Analysis of Materials, ed. N. S. McIntyre, ASTM STP 643 (1977), p. 5.

13. C. S. Fadley, in Electron Spectroscopy: Theory, Techniques and Applications, Vol. 2, eds. C. R. Brundle and A. D. Baker, Academic Press, New York (1978), p. 1.

14. M. P. Seah and W. A. Dench SIA, Surf. Interface Anal. 1, 2 (1979).

15. L. V. Phillips, L. Salvati, W. J. Carter, and D. M. Hercules, in Quantitative Surface Analysis of Materials, ed. N. S. McIntyre, ASTM STP 643 (1977), p. 47.

16. C. Palache, H. Berman, and C. Frondel, Dana's System of Minerology, Vol. 1, John Wiley and Sons, New York (1944), p. 329.

LABORATORY OPERATIONS

The Laboratory Operations of The Aerospace Corporation is conducting experimental and theoretical investigations necessary for the evaluation and application of scientific advances to new military space systems. Versatility and flexibility have been developed to a high degree by the laboratory personnel in dealing with the many problems encountered in the nation's rapidly developing space systems. Expertise in the latest scientific developments is vital to the accomplishment of tasks related to these problems. The laboratories that contribute to this research are:

Aerophysics Laboratory: Launch vehicle and reentry fluid mechanics, heat transfer and flight dynamics; chemical and electric propulsion, propellant chemistry, environmental hazards, trace detection; spacecraft structural mechanics, contamination, thermal and structural control; high temperature thermomechanics, gas kinetics and radiation; cw and pulsed laser development including chemical kinetics, spectroscopy, optical resonators, beam control, atmospheric propagation, laser effects and countermeasures.

Chemistry and Physics Laboratory: Atmospheric chemical reactions, atmospheric optics, light scattering, state-specific chemical reactions and radiation transport in rocket plumes, applied laser spectroscopy, laser chemistry, laser optoelectronics, solar cell physics, battery electrochemistry, space vacuum and radiation effects on materials, lubrication and surface phenomena, thermionic emission, photosensitive materials and detectors, atomic frequency standards, and environmental chemistry.

Computer Science Laboratory: Program verification, program translation, performance-sensitive system design, distributed architectures for spaceborne computers, fault-tolerant computer systems, artificial intelligence and microelectronics applications.

Electronics Research Laboratory: Microelectronics, GaAs low noise and power devices, semiconductor lasers, electromagnetic and optical propagation phenomena, quantum electronics, laser communications, lidar, and electro-optics; communication sciences, applied electronics, semiconductor crystal and device physics, radiometric imaging; millimeter wave, microwave technology, and RF systems research.

Materials Sciences Laboratory: Development of new materials: metal matrix composites, polymers, and new forms of carbon; nondestructive evaluation, component failure analysis and reliability; fracture mechanics and stress corrosion; analysis and evaluation of materials at cryogenic and elevated temperatures as well as in space and enemy-induced environments.

Space Sciences Laboratory: Magnetospheric, auroral and cosmic ray physics, wave-particle interactions, magnetospheric plasma waves; atmospheric and ionospheric physics, density and composition of the upper atmosphere, remote sensing using atmospheric radiation; solar physics, infrared astronomy, infrared signature analysis; effects of solar activity, magnetic storms and nuclear explosions on the earth's atmosphere, ionosphere and magnetosphere; effects of electromagnetic and particulate radiations on space systems; space instrumentation.

END

FILMED

12-85

DTIC